# Size-Controllable and Low-Cost Fabrication of Graphene Quantum Dots Using Thermal Plasma Jet

Juhan Kim and Jung Sang Suh*

Nano Materials Laboratory, Department of Chemistry, Seoul National University, Kwanakro 1, Kwanakgu, Seoul 151-747, Republic of Korea

ABSTRACT We report a size-controllable and low-cost fabrication method of graphene quantum dots (GQDs) using a thermal plasma jet. A carbon atomic beam was generated by injecting a large amount (2.5 L/min) of ethylene gas continuously into Ar plasma. The beam was then flowed through a carbon tube (5—20 cm in length) attached to the anode and then dispersed into a chamber. Carbon
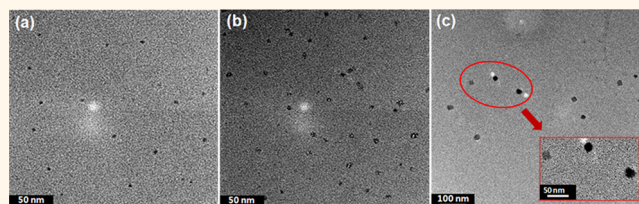
materials including GQDs were made by a gas phase collision reaction. The production rate of carbon soot was 40 g/h for a 2.5 L/min injection rate. Almost all of the carbon soot dispersed in ethanol by sonication, while isolated GQDs were dispersed in ethanol by stirring with a stirring rod. The weight percent of GQDs in carbon soot, based on the amount extracted in ethanol, was about 10%. This means that the production rate of GQDs was about 4 g/h. The average size of GQDs, with a relatively narrow size distribution, was controlled by varying the length of the carbon tube attached. It was about 10, 14, and 19 nm when the length was 5, 10, and 20 cm, respectively. The electric structure based on the photoluminescence data of our GQDs had a singlet ground state and was in good agreement with that of carbyne. Our GQDs will disperse in organic solvents such as toluene, but not in water. The dispersion properties also support that our GQDs have carbyne-like edges. We proposed that the PL peaks observed can be attributed to electronic transitions between energy levels of the GQDs having carbyne-like edges.

KEYWORDS: graphene quantum dots · thermal plasma jet · mass production · size-controllable fabrication · low-cost fabrication · carbyne-like edges · photoluminescence

G raphene,[1] a two-dimensional material of sp[2]-hybridized carbon atoms, has generated a great deal of interest due to its extraordinary properties[2—5] and potential applications.[6—10] However, there are two serious drawbacks regarding its application. One is that graphene is a zero-band-gap semiconductor, which limits its electronic and optoelectronic application.[11] The other is that graphene is not dispersible in common solvents. However, it is known that the properties of graphene can be affected by the morphology of graphene sheets, including their size, shape, and thickness.[12—14] Graphene quantum dots (GQDs), which are graphene sheets smaller than 100 nm, possess strong quantum confinement and edge effects.[15] Confinement allows the band gap of GQDs to be controlled by modulating their size, while edge effects allow dispersion in solvents such as ethanol. These properties of GQDs make them excellent materials for the construction of nano-scaled optical and electronic devices.[16—20]

GQDs have been prepared mainly by top-down and bottom-up methods. The cutting of graphene sheets,[15] graphene oxide sheets,[14,18,21,22] or carbon fibers[17] or using a self-assembled block copolymer[23] corresponds to a top-down method, while cyclodehydrogenation of polyphenylene precursors,[24,25] self-assembling of aromatic carbons followed by pyrolysis,[26] and the microwave-assisted hydrothermal method[27] correspond to a bottom-up method. Cage-opening of fullerenes[28] may be categorized as a third method. However, these methods have some drawbacks including size-controllable fabrication, mass production, and low-cost production.

Recently we have developed a method to fabricate graphene using a thermal plasma jet.[29] In this fabrication, a carbon atomic beam is generated by continuously injecting a very small amount of ethanol as a carbon source into Ar plasma; the beam is then flowed through a carbon tube attached to the anode and then collides with
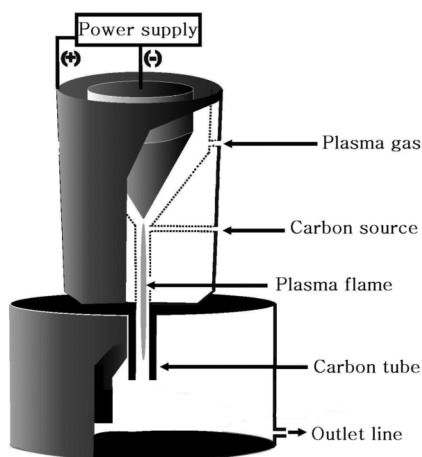
Figure 1. Schematic of the thermal plasma jet system for the production of GQDs.
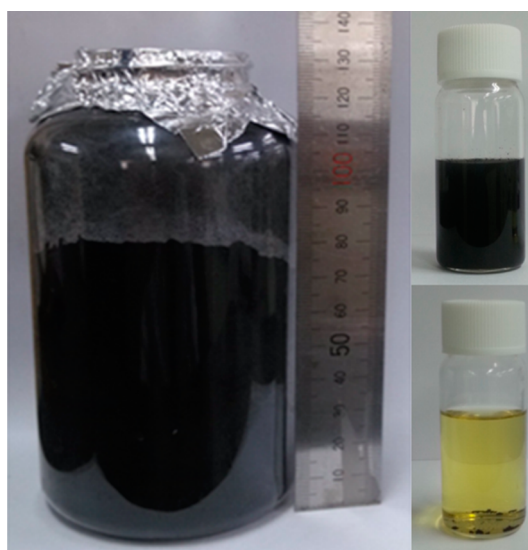

Figure 2. Pictures of raw carbon soot and two dispersing solutions of carbon soot in ethanol. The carbon soot was produced by injecting ethylene continuously (2.5 L/min), with a carbon tube (20 cm in length) attached to the anode. The black solution was prepared by sonicating carbon soot in ethanol, while the pale yellow solution by stirring with a stirring rod.

the graphite plate that was placed in the path of the beam, perpendicular to the attached carbon tube. The fabricated graphene is very pure and shows relatively good crystalline structure. Graphene was made by an epitaxial growth on the graphite plate when a carbon atomic beam, having a proper energy, collided with a graphite plate. The size of graphene was several hundred nanometers, and the graphene did not disperse in common solvents.

Herein, we report a size-controllable and low-cost GQD fabrication method using a thermal plasma jet. A large amount of ethylene gas (2.5 L/min) as carbon source was injected continuously into Ar plasma to generate a carbon atomic beam (see Figure 1). The beam was then flowed through a carbon tube attached to the anode and then dispersed into a chamber. Carbon materials including GQDs were made by a gas phase collision reaction during flow through the attached carbon tube. The production rate of GQDs was about 4g/h. The average size of GQDs, with a relatively narrow size distribution, was controlled by varying the length of the attached carbon tube.

RESULTS AND DISCUSSION

We produced carbon soot by injecting ethylene gas continuously (at a rate of 2.5 L/min) into Ar plasma and attaching a carbon tube (5, 10, or 20 cm in length) to the anode. Figure 2 shows pictures of raw carbon soot produced by attaching a 20 cm carbon tube and its dispersing solutions. The production rate of carbon soot was 0.67 g/min (or 40 g/h). The black solution was prepared by sonicating carbon soot in ethanol, and the pale yellow solution by stirring with a stirring rod. This pale yellow solution emitted strong luminescence. *Via* sonication almost all of the carbon soot dispersed in ethanol, while by stirring with a stirring rod about 10% of the carbon soot was dispersed in ethanol. Both dispersing solutions were very stable for several months. Yellow solutions were obtained by dispersing

carbon soot in toluene, pyridine, dimethyl sulfoxide (DMSO), and ethanol with a stirring rod. Among these, the toluene solution showed the brightest color. However, in water a very small portion of carbon soot was dispersed, even by sonication.

Figure 3 shows the HRTEM images of onion-type materials and GQDs. In Figure 3a, onion-type carbon materials having contour-like fringes are observed. The TEM sample for onion-type materials was prepared by dispersing carbon soot, which was produced by attaching a 20 cm carbon tube, in ethanol by sonication. The dominant species of carbon soot were onion-type materials. Figure 3b shows the high-resolution TEM (HRTEM) image of a GQD, which shows the high crystallinity of GQDs, with lattice parameter 0.32 nm, and (002) lattice fringes of graphene. The corresponding fast Fourier transform (FFT) pattern is shown in the inset of Figure 3b. It shows a hexagonal pattern without any satellite spots. Single-layer graphene shows no satellite spots.[30] Therefore, we can conclude that our GQDs are single-layered. This is supported by the atomic force microscopy (AFM) analysis of our GQDs (see Figure S1). The height profile of the line in Figure S1 shows that the thickness of the GQDs is less than 1 nm, which is in good agreement with the reported value for single-layered graphene.[31] The TEM and AFM samples for GQDs were prepared by dispersing carbon soot in ethanol by stirring with a stirring rod.

Figure 4 shows the TEM images of GQDs extracted from three kinds of carbon soot produced by attaching a carbon tube (5, 10, or 20 cm in length) to the anode. These TEM samples were prepared by stirring three kinds of carbon soot in ethanol with a stirring rod.
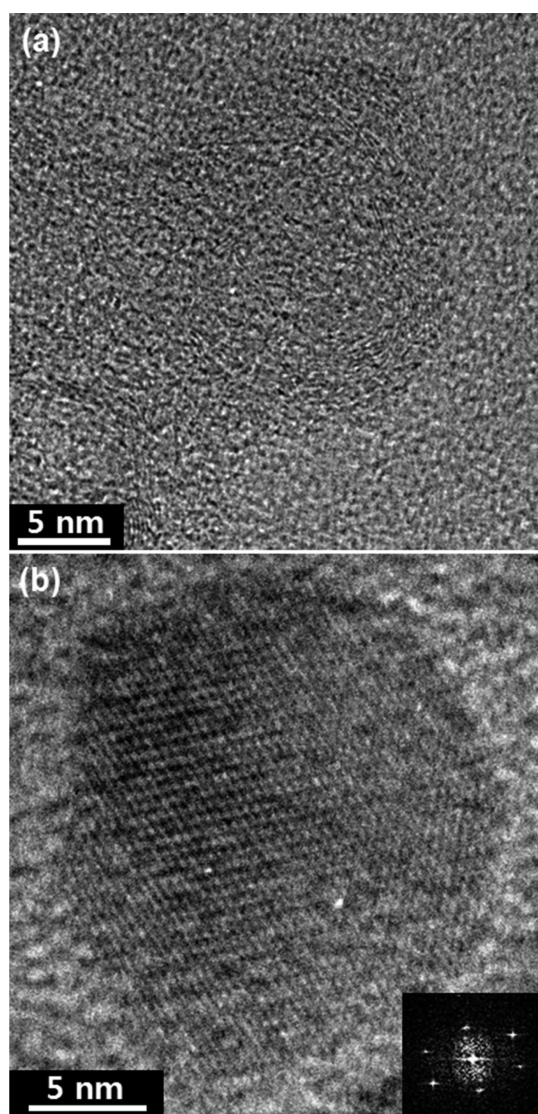
Figure 3. HRTEM images of (top) onion-type carbon materials and (bottom) GQDs. Inset is the 2D FFT pattern.

No onion-type carbon materials are observed. This means that, when carbon soot was dispersed in ethanol using a stirring rod, only GQDs were dispersed in the ethanol. It is a very simple and low-cost process. The weight percent of GQDs in carbon soot, based on the amount extracted in ethanol, was about 10%.

According to the analysis of the TEM images, the size of the GQDs extracted from carbon soot produced by attaching a 5 cm carbon tube was in the range of 7 to 11 nm (see Figure 4a), while it was in the range of 11 to 15 nm for a 10 cm tube (see Figure 4b) and in the range 17 to 23 nm for a 20 cm tube (see Figure 4c). The size distributions are shown in Figure S2. The average sizes were about 10, 14, and 19 nm. The absolute quantum yields of these GQDs were 13.5%, 12.2%, and 9.6%, respectively (see Table S1). The average size of GQDs increased with increasing anode-attached carbon tube length. Under high ethylene injection rates, collisions between carbon atoms would take place mostly during
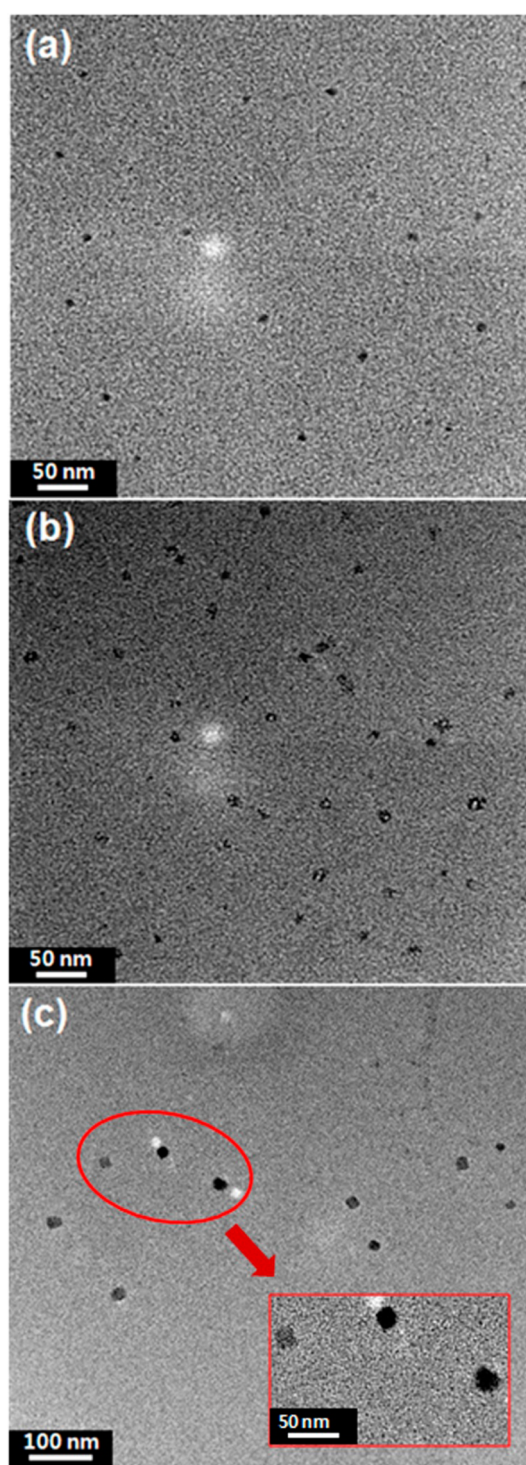

Figure 4. TEM images of GQDs extracted from three kinds of carbon soot produced by attaching carbon tubes of three different lengths to the anode. The length of the carbon tube attached was (a) 5, (b) 10, and (c) 20 cm. The average size of GQDs was about (a) 10 nm, (b) 14 nm, and (c) 19 nm.

flow through the carbon tube. Since the atomic beam was dispersed into a chamber after passing through the tube, collision reactions could take place only during flow through the carbon tube. Therefore, the reaction time would increase linearly when increasing the length of the tube. Increasing the reaction time

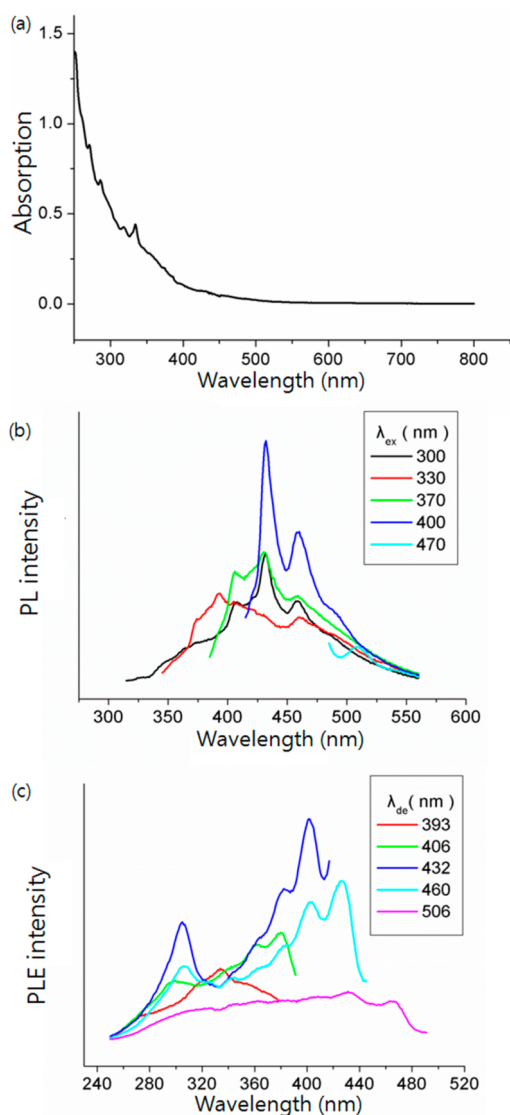would also increase the total number of collisions. Therefore, it is concluded that the average size of GQDs

Figure 5. (a) UV−vis absorption, (b) PL emission, and (c) PL excitation spectra of 19 nm GQD suspension in ethanol. The legends in (b) are the excitation wavelengths, and those in (c) are the detection wavelengths.

could be controlled by varying the length of the carbon tube attached to the anode.

UV−vis absorption, excitation-dependent photoluminescence (PL), and emission-dependent PL excitation (PLE) spectra of three GQD suspensions in ethanol are shown in Figures 5, S3, and S4. The average sizes of GQDs in the three suspensions were 10, 14, and 19 nm. The GQD suspensions show a broad UV−vis absorption with shoulder-type peaks at 270, 280, 318, and 330 nm. Relative absorption intensity slightly increased when the average size of suspended GQDs increased (see Figure S3). Three suspensions show almost the same excitation-dependent PL and emission-dependent PLE spectra except their relative intensity (see Figure S4). The same peak positions suggest that they share the same luminescence origin. The PL peaks were observed near 375, 393, 406, 430, 460, 490, and 506 nm. The PL peak near 490 nm was very weak, and the peak centered at 506 nm was observed only by excitation with a relatively low energy light. The PLE spectra were measured by detecting at 393, 406, 432, 460, and 506 nm. For the PLE spectrum with the detection wavelength of 460 nm (2.70 eV), there are three strong absorption peaks at 426.4 (2.91 eV), 402.7 (3.08 eV), and 306.1 nm (4.05 eV) and three weak ones at near 380.7 (3.26 eV), 343.2 (3.61 eV), and 361.6 nm (3.43 eV). For the detection wavelength of 506 nm (2.45 eV), there are two weak peaks at 466.9 (2.66 eV) and 432.4 nm (2.87 eV). The absorption energies measured from the PLE spectra are summarized in Table 1, and a schematic of the electric structure is shown in Figure 6.

The electric structure consists of seven levels. The relative energy levels except the HOMO were determined simply by arranging the absorption energy data. Determination of the HOMO will be discussed below. It should be mentioned that the energy gaps shown in Figure 6 are based on the data of electronic transitions accompanied by vibrational transitions, and these values are not pure electronic transition energies.[32] The HOMO−HOMO−1 gap has been determined by assuming that the states reached by absorption of the

TABLE 1. Absorption Energies Measured from the PLE Spectra Shown in Figure 5

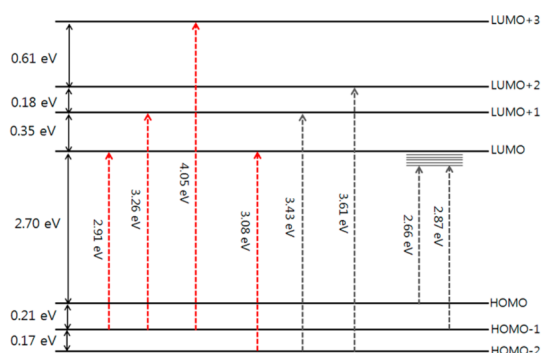| λ_{de}	$\sim\lambda_{ab}$							
	470 nm	430 nm	400 nm	380 nm	360 nm	340 nm	310 nm	290 nm
506 nm (2.45 eV)	467.8 nm (2.66 eV) w	432.4 nm (2.87 eV) w						
460 nm (2.70 eV)		426.4 nm (2.91 eV) vs	402.7 nm (3.08 eV) s	380.7 nm (3.26 eV) w	361.6 nm (3.43 eV) w	343.2 nm (3.61 eV) w	306.1 nm (4.05 eV) s	
432 nm (2.87 eV)			402.4 nm (3.08 eV) vs	381.4 nm (3.25 eV) s			305.5 nm (4.06 eV) vs	
406 nm (3.05 eV)				379.5 nm (3.27 eV) s	361.5 nm (3.43 eV) w			293.8 nm (4.22 eV) w
393 nm (3.16 eV)						334.0 nm (3.71 eV) m		

Figure 6. Schematic of the electric structure of our GQDs based on the PLE data shown in Figure 5. The HOMO and LUMO+2 are singlet, and the others are triplet. The strong PLE transitions are shown in red.

lights of 2.66 eV from the HOMO and 2.87 eV from the HOMO−1 are the same state. The energy difference is 0.21 eV. Therefore, the HOMO lies 0.21 eV above the HOMO−1. Some observed energies, particularly for the energies of very weak absorptions, are slightly different from the energy gaps shown in the electronic structure, which was based on mainly the data measured from the strong absorption peaks. The weak absorptions are mainly due to spin-forbidden transitions, while the strong absorptions spin-allowed ones. Their transition mechanisms are different, and the vibrational levels involved in a spin-forbidden transition are different from those in a spin-allowed transition.[32] Therefore, when two transitions take place between any given two electric states, the center position of a weak absorption peak could be slightly different from that of the strong one. Radovic and Bockrath proposed that for the oxygen-free edges of graphene sheets or quantum dots, free zigzag sites are carbene-like, with a triplet ground state being most common, whereas free armchair sites are carbyne-like, with a singlet ground state being most common.[33] The electronic structures of both types have seven energy levels, and two of them are singlet and the others are triplet.[33] In the PL spectrum with 400 nm excitation, there is a weak shoulder near 490 nm (2.53 eV), whose energy is slightly lower than the HOMO−LUMO gap (2.7 eV). The weak luminescence is mainly due to the spin-forbidden transition. This means that HOMO and LUMO have a different multiplicity. For the PLE spectrum with the detection wavelength of 432 nm (2.87 eV), there are three strong absorption peaks at 402.4 (3.08 eV), 381.4 (3.25 eV), and 305.5 nm (4.06 eV). These energies correspond to the energy differences between HOMO−2 and LUMO, HOMO−1 and LUMO+1, and HOMO−1 and LUMO+3, respectively. Since strong peaks are mainly due to spin-allowed transitions, the HOMO−1, HOMO−2, LUMO, LUMO+1, and LUMO+3 have the same multiplicity. The energy difference between HOMO−2 and LUMO+2 levels is 3.61 eV, which is well distinguished from other energy values.

The absorption peak at 343 nm (3.61 eV) is very weak in all the PLE spectra except the one with the detection wavelength of 393 nm (3.16 eV). The relatively strong PL peak centered at 393 nm (3.16 eV) may correspond to the luminescence from LUMO+2 to HOMO, whose gap is 3.23 eV. A strong luminescence could take place when the HOMO and LUMO+2 have the same multiplicity. By the calculation of Radovic and Bockrath, among seven levels two of them are singlet and the others are triplet.[33] Therefore, it is concluded that HOMO and LUMO+2 are singlet and the others are triplet. Since the HOMO is singlet, our GQDs may have carbyne-like edges.[33] The H-free armchair sites of GQDs become carbyne-like edges when triple bonds are made by rehybridizing. Therefore, we propose that the PL peaks observed can be attributed to electronic transitions between energy levels of the GQDs having carbyne-like edges. Our GQDs dispersed in organic solvents such as toluene, but did not disperse in water. Carbyne is o-benzyne, which is a nonpolar compound and does not dissolve in water. The dispersion properties of our GQDs also support that they have carbyne-like edges. The PL and PLE spectra of three suspensions whose average GQD sizes were 10, 14, and 19 nm were almost the same except for their relative intensity (see Figures S3). With a decrease in the average size of GQDs, the relative intensity of the PLE peaks near 300 nm was decreased. Also, the relative intensity of PL spectra excited by 300 and 330 nm light was decreased. These behaviors seem to be due to a quantum size effect. However, further studies are needed to gain a better understanding of the cause of these behaviors.

It is known that the PL characteristic of GQDs is critically affected by the content of oxygen.[34] In principle, oxygen is not contained in our fabrication, since only Ar and ethylene gases have been added into a plasma system as the plasma gas and carbon source, respectively. According to the energy-dispersive X-ray spectroscopy (EDS) analysis of carbon soot including GQDs, no oxygen was observed from carbon soot not exposed to air, while oxygen (3.60 atomic %) was observed from carbon soot exposed to air for about 30 min (see Figure S5). X-ray photoelectron spectroscopy (XPS) was performed to determine the composition of our GQDs (see Figure S6). The measured spectra could be deconvoluted into four surface components, corresponding to sp^2 (C=C) at binding energy of 284.5 eV, sp^3 (C−C and C−H) at 285.5 eV, C−OH at 286.6 eV, and O=C−OH at 288.6 eV. The bands corresponding to C−OH and O=C−OH were relatively weak. Oxygen might be included during the specimen preparation process, since the fresh carbon soot did not contain oxygen.

This fabrication method of GQDs is basically different from our previous fabrication method[29] of graphene. In our previous method, graphene is made on the surface of the graphite plate by an epitaxial growth

when the carbon atoms of a carbon atomic beam collide with the graphite plate placed in the path of the carbon atomic beam. However, GQDs are made by a gas phase collision reaction, since no graphite plate is placed in the path of the carbon atomic beam. The injection rate of ethylene was 2.5 L/min, which is relatively very high. In the previous method, the injection rate of ethanol was 0.1 mL/min, which corresponds to 40 mL/min in the gas phase.[29] For one's information, the injection rate of Ar plasma gas was 13.5 L/min. By a simple calculation, the proportion of carbon atoms in the atomic beam is roughly 17.5%, since two carbon and four hydrogen atoms are generated when an ethylene molecule is atomized. Therefore, under our experimental conditions, the collisions between carbon atoms might take place heavily during flow through the attached carbon tube.

Our method is a relatively low-cost process. Our thermal plasma system including a dc power supply is a relatively inexpensive setup, and ethylene is a cheap chemical. Also, the total electrical consumption is not substantial. Our fabrication is a continuous process. The production rate of carbon soot was 0.67 g/min (or 40 g/h) for a 2.5 L/min injection rate of ethylene gas, and the weight percent of GQDs in carbon soot, based on the amount extracted in ethanol, was about 10%. By simple calculation, a plasma system could produce 40 g of GQDs per day by assuming 10 h operation. This means that mass production of GQDs could be possible if we operated many plasma systems. In the fabrication of our GQDs, no chemical treatment was involved except for dispersion in ethanol, which is a mild solvent. Also, the fabrication temperature was relatively high, and it is known that the crystallinity of carbon materials such as carbon nanotubes increases with increasing fabrication temperature.[35,36] Therefore, our GQDs ought to have a good crystallinity. A Raman spectrum of our GQDs is shown in Figure S7. The G band near 1596 cm^{-1} was stronger than the D band near 1353 cm^{-1}. The D band is known due to the presence of structural disorder in the graphene sheets. A higher G/D intensity ratio indicates better crystallinity of the GQDs. However, the edges are always seen as defects, and the portion of edges increases with decreasing GQD size. Generally, GQDs show a relatively low G/D intensity ratio.[14,17,22,34] The intensity ratio of our GQDs was relatively high, 1.6.

CONCLUSIONS

We have developed a size-controllable and low-cost GQD fabrication method using a thermal plasma jet. A large amount of ethylene gas was injected continuously into Ar plasma to generate a carbon atomic beam. The beam was then flowed through a carbon tube attached to the anode and then dispersed into a chamber. Carbon materials including GQDs were made by a gas phase collision reaction. The production rate of carbon soot was 40 g/h for a 2.5 L/min injection rate of ethylene. We could extract isolated GQDs from carbon soot simply by dispersing it in ethanol using a stirring rod. The weight percent of GQDs in carbon soot, based on the amount extracted in ethanol, was about 10%. We could control the average size of GQDs, with a relatively narrow size distribution, by varying the length of the carbon tube attached. Our method is a size-controllable, low-cost, and mass producible process. The electric structure based on the PL and PLE data has a singlet ground state, and it is in good agreement with that of carbyne. Our GQDs were dispersed in organic solvents such as toluene, but did not disperse in water. These properties also support that our GQDs have carbyne-like edges. The PL peaks observed are attributed to electronic transitions between energy levels of the GQDs having carbyne-like edges.

EXPERIMENTAL SECTION

The thermal plasma jet system used here is basically the same one as reported,[29−31] but no graphite plate was placed in the path of the plasma gas, nor was a catalyst source injected (see Figure 1). Carbon tubes of various lengths (5−20 cm; 2 cm in diameter) were attached to the anode. Thermal plasma of Ar (99.999%, at the injection flow rate of 13.5 L per min) was generated by applying a high voltage of ∼3 kV between a zirconium-containing tungsten cathode and a copper anode. The thermal plasma jet for generating a carbon atomic beam was operated by a dc of ∼200 A and 60 V. A plasma jet with a value close to sound velocity flowed into a Cu nozzle (6 mm in inner diameter), then continued through an attached carbon tube. Ethylene gas was introduced continuously (2.5 L per min) as a carbon source into the torch using a gas flow meter. Carbon soot produced was dispersed in ethanol by stirring with a stirring rod. In this case, isolated GQDs were dispersed in ethanol. GQDs were analyzed by using a scanning electron microscope (SEM; JEOL Ltd., JSM6700F (10 kV)) and a high-resolution transmission electron microscope (JEOL, JEM-3000F (300 kV)). AFM images were taken using a PSIA (XE-150) atomic force microscope. UV−vis spectra were recorded on a UV-3600 spectrophotometer (Scinco, NEOSYS-2000). PL and PLE spectra were obtained using a homemade spectrophotometer. Absolute quantum yield was measured by absolute PL quantum yield measurement system QE-1200 (Otsuka Electronics).

suspensions in ethanol, SEM images and EDS spectra of carbon soot, XPS C 1s spectrum of GQDs, Raman spectrum of GQDs. This material is available free of charge *via* the Internet at http://pubs.acs.org.

REFERENCES AND NOTES

1. Geim, A. K.; Novoselov, K. S. The Rise of Graphene. *Nat. Mater.* **2007**, *6*, 183–191.
2. Novoselov, K. S.; Jiang, Z.; Zhang, Y.; Morozov, S. V.; Stormer, H. L.; Zeitler, U.; Maan, J. C.; Boebinger, G. S.; Kim, P.; Geim, A. K. Room-Temperature Quantum Hall Effect in Graphene. *Science* **2007**, *315*, 1379.
3. Zhang, Y. B.; Tan, Y. W.; Stormer, H. L.; Kim, P. Experimental Observation of the Quantum Hall Effect and Berry's Phase in Graphene. *Nature* **2005**, *438*, 201–204.
4. Novoselov, K. S.; Geim, A. K.; Morozov, S. V.; Jiang, D.; Katsnelson, M. I.; Grigorieva, I. V.; Dubonos, S. V.; Firsov, A. A. Two-Dimensional Gas of Massless Dirac Fermions in Graphene. *Nature* **2005**, *438*, 197–200.
5. Katsnelson, M. I.; Novoselov, K. S.; Geim, A. K. Chiral Tunnelling and the Klein Paradox in Grapheme. *Nat. Phys.* **2006**, *2*, 620–625.
6. Areshkin, D. A.; Gunlycke, D.; White, C. T. Ballistic Transport in Graphene Nanostrips in the Presence of Disorder: Importance of Edge Effects. *Nano Lett.* **2007**, *7*, 204–210.
7. Liao, L.; Bai, J.; Qu, Y.; Huang, Y.; Duan, X. Highly Ordered Graphene for Two Dimensional Electronics. *Appl. Phys. Lett.* **2006**, *89*, 143106.
8. Watcharotone, S.; Dikin, D. A.; Stankovich, S.; Piner, R.; Jung, I.; Dommett, G. H. B.; Evmenenko, G.; Wu, S. E.; Chen, S. F.; Liu, C. P.; *et al.* Graphene-Silica Composite Thin Films as Transparent Conductors. *Nano Lett.* **2007**, *7*, 1888–1892.
9. Wang, X.; Zhi, L. J.; Müllen, K. Transparent, Conductive Graphene Electrodes for Dye-Sensitized Solar Cells. *Nano Lett.* **2008**, *8*, 323–327.
10. Schedin, F.; Geim, A. K.; Morozov, S. V.; Hill, E. W.; Blake, P.; Katsnelson, M. I.; Novoselov, K. S. Detection of Individual Gas Molecules Adsorbed on Graphene. *Nat. Mater.* **2007**, *6*, 652–655.
11. Novoselov, K. S.; Geim, A. K.; Morozov, S. V.; Jiang, D.; Zhang, Y.; Dubonos, S. V.; Grigorieva, I. V.; Firsov, A. A. Electric Field Effect in Atomically Thin Carbon Films. *Science* **2004**, *306*, 666–669.
12. Li, X. L.; Wang, X. R.; Zhang, L.; Lee, S. W.; Dai, H. J. Chemically Derived Ultrasmooth Graphene Nanoribbon Semiconductors. *Science* **2008**, *319*, 1229–1232.
13. Kosynkin, D. V.; Higginbotham, A. L.; Sinitskii, A.; Lomeda, J. R.; Dimiev, A.; Price, B. K.; Tour, J. M. Longitudinal Unzipping of Carbon Nanotubes to Form Graphene Nanoribbons. *Nature* **2009**, *458*, 872–877.
14. Pan, D. Y.; Zhang, J. C.; Li, Z.; Wu, M. H. Hydrothermal Route for Cutting Graphene Sheets into Blue-Luminescent Graphene Quantum Dots. *Adv. Mater.* **2010**, *22*, 734–738.
15. Ponomarenko, L. A.; Schedin, F.; Katsnelson, M. I.; Yang, R.; Hill, E. W.; Novoselov, K. S.; Geim, A. K. Chaotic Dirac Billiard in Graphene Quantum Dots. *Science* **2008**, *320*, 356–358.
16. Ritter, K. A.; Lyding, J. W. The Influence of Edge Structure on the Electronic Properties of Graphene Quantum Dots and Nanoribbons. *Nat. Mater.* **2009**, *8*, 235–242.
17. Peng, J.; Gao, W.; Gupta, B. K.; Liu, Z.; Romero-Aburto, R.; Ge, L.; Song, L.; Alemany, L. B.; Zhan, X.; Gao, G.; *et al.* Graphene Quantum Dots Derived from Carbon Fibers. *Nano Lett.* **2012**, *12*, 844–849.
18. Gupta, V.; Chaudhary, N.; Srivastava, R.; Sharma, G. D.; Bhardwaj, R.; Chand, S. Luminscent Graphene Quantum Dots for Organic Photovoltaic Devices. *J. Am. Chem. Soc.* **2011**, *133*, 9960–9963.
19. Zhu, S. J.; Zhang, J. H.; Qiao, C. Y.; Tang, S. J.; Li, Y. F.; Yuan, W. J.; Li, B.; Tian, L.; Liu, F.; Hu, R.; *et al.* Strongly Green-Photoluminescent Graphene Quantum Dots for Bioimaging Applications. *Chem. Commun.* **2011**, *47*, 6858–6860.
20. Cheng, H.; Zhao, Y.; Fan, Y.; Xie, X.; Qu, L.; Shi, G. Graphene-Quantum-Dot Assembled Nanotubes: A New Platform for Efficient Raman Enhancement. *ACS Nano* **2012**, *6*, 2237–2244.
21. Shen, J. H.; Zhu, Y. H.; Chen, C.; Yang, X. L.; Li, C. Z. Facile Preparation and Upconversion Luminescence of Graphene Quantum Dots. *Chem. Commun.* **2011**, *47*, 2580–2582.
22. Li, Y.; Hu, Y.; Zhao, Y.; Shi, G. Q.; Deng, L.; Hou, Y. B.; Qu, L. T. An Electrochemical Avenue to Green-Luminescent Graphene Quantum Dots as Potential Electron-Acceptors for Photovoltaics. *Adv. Mater.* **2011**, *23*, 776–780.
23. Lee, J.; Kim, K.; Park, W. I.; Kim, B. H.; Park, J. H.; Kim, T. H.; Bong, S.; Kim, C. H.; Chae, G.; Jun, M.; *et al.* Uniform Graphene Quantum Dots Patterned from Self-Assembled Silica Nanodots. *Nano Lett.* **2012**, *12*, 6078–6083.
24. Wu, J. S.; Pisula, W.; Müllen, K. Graphenes as Potential Material for Electronics. *Chem. Rev.* **2007**, *107*, 718–747.
25. Yan, X.; Cui, X.; Li, L. S. Synthesis of Large, Stable Colloidal Graphene Quantum Dots with Tunable Size. *J. Am. Chem. Soc.* **2010**, *132*, 5944–5945.
26. Liu, R.; Wu, D.; Feng, X.; Müllen, K. Bottom-Up Fabrication of Photoluminescent Graphene Quantum Dots with Uniform Morphology. *J. Am. Chem. Soc.* **2011**, *133*, 15221–15223.
27. Tang, L.; Ji, R.; Cao, X.; Lin, J.; Jiang, H.; Li, X.; Teng, K. S.; Luk, C. M.; Zeng, S.; Hao, J.; *et al.* Deep Ultraviolet Photoluminescence of Water-Soluble Self-Passivated Graphene Quantum Dots. *ACS Nano* **2012**, *6*, 5102–5110.
28. Lu, J.; Yeo, P. S. E.; Gan, C. K.; Wu, P.; Loh, K. P. Transforming C_{60} Molecules into Graphene Quantum Dots. *Nat. Nanotechnol.* **2011**, *6*, 247–252.
29. Kim, J.; Heo, S. B.; Gu, G. H.; Suh, J. S. Fabrication of Graphene Flakes Composed of Multi-Layer Graphene Sheets Using a Thermal Plasma Jet System. *Nanotechnology* **2010**, *21*, 095601.
30. Ci, L.; Song, L.; Jin, C.; Jariwala, D.; Wu, D.; Li, Y.; Srivastava, A.; Wang, Z. F.; Storr, K.; Balicas, L.; *et al.* Atomic Layers of Hybridized Boron Nitride and Graphene Domains. *Nat. Mater.* **2010**, *9*, 430–435.
31. Gupta, A.; Chen, G.; Joshi, P.; Tadigadapa, S.; Eklund, P. C. Raman Scattering from High-Frequency Phonons in Supported n-Graphene Layer Films. *Nano Lett.* **2006**, *6*, 2667–2673.
32. Hollas, J. M., Ed. *Modern Spectroscopy*; John Wiley & Sons, Ltd, 2004.
33. Radovic, L. R.; Bockrath, B. On the Chemical Nature of Graphene Edges: Origin of Stability and Potential for Magnetism in Carbon Materials. *J. Am. Chem. Soc.* **2005**, *127*, 5917–5927.
34. Liu, F.; Jang, M. H.; Ha, H. D.; Kim, J. H.; Cho, Y. H.; Seo, T. S. Facile Synthetic Method for Pristine Graphene Quantum Dots and Graphene Oxide Quantum Dots: Origin of Blue and Green Luminescence. *Adv. Mater.* **2013**, *25*, 3657–3662.
35. Hahn, J.; Jung, H. Y.; Kang, D. W.; Yoo, J. E.; Suh, J. S. Selective Synthesis of High-Purity Carbon Nanotubes by Thermal Plasma Jet. *Carbon* **2004**, *42*, 3024–3027.
36. Hahn, J.; Heo, S. B.; Suh, J. S. Catalyst Free Synthesis of High Quality Carbon Nanotubes Using Thermal Plasma Jet. *Carbon* **2005**, *43*, 2638–2641.